JBC RESEARCH ARTICLE

A small molecule toll-like receptor antagonist rescues α-synuclein fibril pathology

Received for publication, February 21, 2022, and in revised form, June 22, 2022 Published, Papers in Press, July 13, 2022,
https://doi.org/10.1016/j.jbc.2022.102260

Jessica Chedid, Adahir Labrador-Garrido, Siying Zhong, Jianqun Gao, Ye Zhao, Gayathri Perera, Woojin S. Kim, Glenda M. Halliday, and Nicolas Dzamko*

From the School of Medical Sciences, Faculty of Medicine and Health and the Brain and Mind Centre, University of Sydney, Camperdown, New South Wales, Australia

Edited by Elizabeth Coulson

The propagation and accumulation of pathological α-synuclein protein is thought to underlie the clinical symptoms of the neurodegenerative movement disorder Parkinson's disease (PD). Consequently, there is significant interest in identifying the mechanisms that contribute to α-synuclein pathology, as these may inform therapeutic targets for the treatment of PD. One protein that appears to contribute to α-synuclein pathology is the innate immune pathogen recognition receptor, toll-like receptor 2 (TLR2). TLR2 is expressed on neurons, and its activation results in the accumulation of α-synuclein protein; however, the precise mechanism by which TLR2 contributes to α-synuclein pathology is unclear. Herein we demonstrate using human cell models that neuronal TLR2 activation acutely impairs the autophagy lysosomal pathway and markedly potentiates α-synuclein pathology seeded with α-synuclein preformed fibrils. Moreover, α-synuclein pathology could be ameliorated with a novel small molecule TLR2 inhibitor, including in induced pluripotent stem cell-derived neurons from a patient with PD. These results provide further insight into how TLR2 activation may promote α-synuclein pathology in PD and support that TLR2 may be a potential therapeutic target for the treatment of PD.

Parkinson's disease (PD) is a progressive debilitating neurodegenerative disease characterized by loss of dopaminergic neurons in the substantia nigra pars compacta and the presence of proteinaceous inclusions in neurons: Lewy bodies (LBs) and Lewy neurites termed collectively Lewy pathologies (1). These inclusions are particularly enriched with the protein α-synuclein and constitute a hallmark for several diseases such as PD, dementia with Lewy bodies, and multiple system atrophy (2). Moreover, missense mutations in the *SNCA* gene encoding the α-synuclein protein are associated with familial PD, and polymorphisms in *SNCA* are associated with an increased risk of sporadic PD (3). The temporal progression of PD shows that the appearance of LBs occurs prior to the death of dopaminergic neurons and spreads in a time-dependent manner starting from the brainstem, then the limbic brain regions and finally arriving at the neocortical regions at later stages of the disease. This progression in the spread of LB strongly correlates with different clinical stages of the disease known as the Braak stages of PD (4). Consequently, the mechanisms underlying α-synuclein accumulation and spreading have been a focal point in PD research.

At least one proposed mechanism for the spread of α-synuclein pathology is receptor-mediated endocytosis *via* toll-like receptor 2 (TLR2). TLRs are activated by recognition of pathogen-associated molecular patterns, originating from various nonself microorganisms, such as parasites, bacteria, viruses, and fungi, as well as damage-associated molecular patterns deriving from tissue damage and following cellular stress (5, 6). Subsequent signaling processes triggered by TLR activation have been highly studied in immune cells and include increased production of proinflammatory cytokines such as tumor necrosis factor α and interleukin 1β. However, at least one member of the TLR family, TLR2, is also expressed by neurons, and increased levels of TLR2 on neurons in PD brain are associated with increased α-synuclein pathology (7). Importantly, activation of the TLR2 pathway in neurons, including primary human neurons derived from induced pluripotent stem cells (iPSCs), results in both TLR2 upregulation and the accumulation of endogenous α-synuclein, modeling the pathology seen in human PD brain (7). Moreover, in preclinical studies, targeting TLR2 has been shown to be a potential disease-modifying treatment for PD (8–11)

Exactly how TLR2 contributes to α-synuclein pathology remains to be elucidated; however, both *in vivo* and *in vitro* studies have indicated that activation of neuronal TLR2 is associated with a blockade of the autophagy-lysosomal pathway (7, 11). Protein clearance by the autophagy-lysosome pathway is particularly important in neurons because they are postmitotic cells, where damaged proteins and organelles are not replaced by mitosis and are therefore required to be constantly cleared to avoid neurotoxicity (12). A number of studies have demonstrated that impaired autophagy can occur prior to the onset of α-synuclein pathology, and drugs which promote autophagy may have therapeutic potential for the treatment of PD (reviewed in ((13–15)). In this study, we further demonstrate how neuronal TLR2 activation impacts on the autophagy/lysosomal system and show that prior TLR2 activation markedly potentiates pathology induced

* For correspondence: Nicolas Dzamko, nicolas.dzamko@sydney.edu.au.

by α-synuclein preformed fibrils (PFFs). Moreover, we show that such pathology can be prevented with a novel small molecule inhibitor of TLR2. These results add to evidence of the interplay between inflammation, autophagy/lysosomal signaling, and α-synuclein in PD and further support that TLR2 is an option for therapeutic intervention.

Results

TLR2 activation inhibits lysosomal degradation prior to accumulation of α-synuclein

Previously it has been shown that neuronal TLR2 associates with the accumulation of α-synuclein (7). To further determine the temporal relationship between TLR2 activation and α-synuclein accumulation, differentiated SH-SY5Y neuroblastoma cells were treated with the TLR2 agonist Pam3CSK4 and levels of α-synuclein, TLR2 and the autophagy markers P62, LC3 and LAMP2A were measured over time. At 4 days posttreatment, levels of TLR2 and P62 had increased significantly compared to baseline; however, there was no significant difference in the levels of α-synuclein at this time (Fig. 1, *A* and *B*). Furthermore, Western blot analysis of LC3 suggested a decrease in LC3II expression at 4 days post Pam3CSK4 treatment (Fig. 1*A*). In contrast, a significant increase in the levels of α-synuclein was seen 8 days post Pam3CSK4 treatment, when levels of TLR2 were declining. Interestingly, LAMP2A, a marker of chaperone-mediated autophagy, was not increased at the 4-days timepoint but was increased at 8 days posttreatment with Pam3CSK4, perhaps indicating a later defect in chaperone-mediated autophagy in association with the accumulation of α-synuclein (Fig. 1*A*). Results obtained by immunoblotting were mimicked by immunofluorescence analysis of α-synuclein and P62, that is an increase in P62 that preceded the accumulation of α-synuclein in Pam3CSK4-treated cells (Fig. 1, *C–F*). Interestingly, the levels of α-synuclein still remained significantly elevated after 12 days of treatment, whereas P62 levels were declining (Fig. 1, *C–F*). Co-staining for both P62 and α-synuclein showed concomitant accumulation of both at 6 days posttreatment with Pam3CSK4 (Fig. S1). To determine if increased P62 was associated with an earlier blockade of autophagy, autophagic flux was assessed in SH-SY5Y using a GFP-RFP-LC3 tandem sensor after 2 days of Pam3CSK4 treatment. In the tandem-sensor assay, autophagosomes with a neutral pH emit both red fluorescent protein (RFP) and GFP fluorescence which results in yellow puncta. When incorporated into autophagolysosomes, only RFP fluorescence is detected due to the GFP signal being quenched by the acidic environment. Autophagic flux within the cell can then be quantified by calculating the GFP/RFP colocalization. The percentage of RFP pixels that colocalized with GFP pixels increased significantly 2-days post treatment with Pam3CSK4, compared to control (Fig. 1*G*). Moreover, the colocalization of GFP/RFP percentage increased significantly in both the Pam3CSK4 and control groups upon further treatment with the lysosomal inhibitor chloroquine, indicating a decrease in autolysosome fusion (Fig. 1*G*). The total number of RFP-positive puncta was not different between groups. However, there was a higher percentage of puncta expressing both GFP and RFP (GFP + RFP+) in the Pam3CSK4-treated group (Mean = 59%) than in the control group (mean = 49%) (Fig. 1*H*).

Neuronal TLR2 activation may prevent lysosomal degradation

To determine whether increased P62 levels following TLR2 activation were associated with a general or specific subtype of autophagy impairment, we also used the mitochondrial marker Mitotracker in combination with Lysotracker and P62 as a readout of mitophagy in control and Pam3CSK4-treated SH-SY5Y cells. No significant difference was measured for Mitotracker intensity between control and Pam3CSK4-treated cells (Fig. 2, *A* and *B*); however, a significant increase was observed in the fraction of Mitotracker colocalizing with both lysotracker (Fig. 2*C*) and P62 (Fig. 2*D*) following Pam3CSK4 treatment. Moreover, the average lysosome size increased significantly in cells treated with Pam3CSK4 for 2 days compared to controls (Fig. 2, *E* and *F*), and the number of lysosomes per cell was also significantly increased in Pam3CSK4-treated cells compared to the controls (Fig. 2*G*). Collectively these results suggest that TLR2 activation in neurons impairs autophagy/lysosomal function, potentially by preventing the fusion of lysosomes with autophagosomes.

TLR2-mediated autophagy blockade is α-synuclein independent

To further demonstrate that TLR2-mediated autophagy inhibition is a cause of α-synuclein accumulation rather than a consequence, α-synuclein-knockout SH-SY5Y cells were generated and treated with Pam3CSK4 at 1 μg/ml for 4 days (Fig. 3*A*). The protein levels of P62 (Fig. 3*B*) and TLR2 (Fig. 3*C*) still increased significantly in TLR2-activated cells compared to nontreated cells, even in the absence of endogenous α-synuclein. Moreover, levels of P62 measured by immunostaining were increased to the same extent in both WT and α-synuclein-knockout SH-SY5Y cells following stimulation with Pam3CSK4 (Fig. 3, *D* and *E*).

TLR2 activation markedly potentiates fibril-mediated α-synuclein pathology in SH-SY5Y cells

A blockade in autophagy is also associated with pathology induced with α-synuclein PFFs (16). Therefore, we investigated whether prior TLR2 activation could potentiate α-synuclein PFF pathology in SH-SY5Y cells. Differentiated SH-SY5Y cells were treated with or without Pam3CSK4 at 1 μg/ml for 4 days, then PFFs were added at 1 μg/ml. After 48 h, cells were fixed, and the levels of α-synuclein and P62 proteins measured. Treating the cells with either Pam3CSK4 or PFF alone significantly increased α-synuclein levels compared to untreated control (Fig. S2). However, following dual stimulation with Pam3CSK4 plus PFF, the levels of α-synuclein and P62 were markedly elevated above untreated controls or Pam3CSK4 or PFF treatment alone (Fig. 4, *A–D*), suggesting a synergistic effect of α-synuclein and TLR2 activation. The

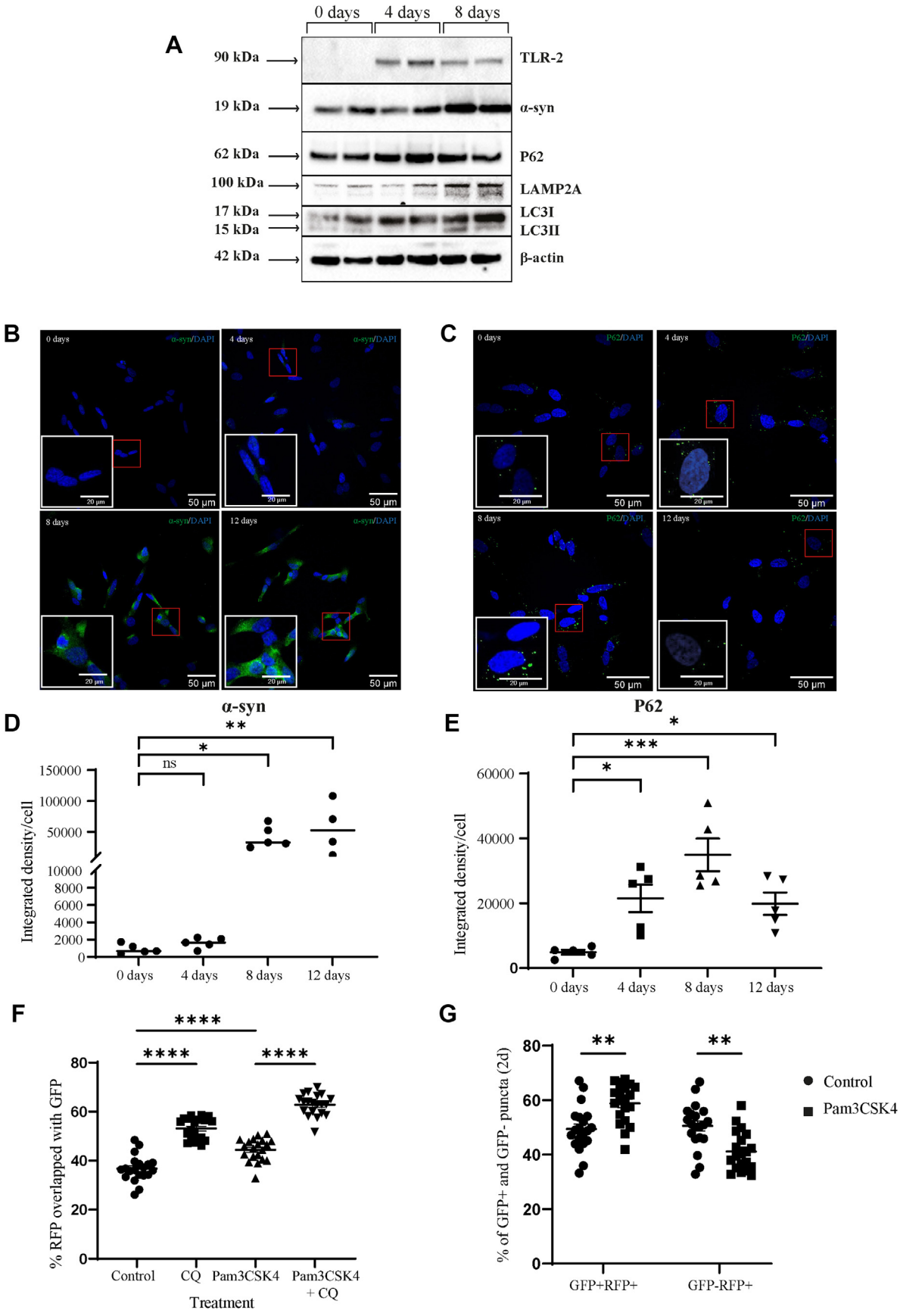

Figure 1. Activation of neuronal toll-like receptor two impairs autophagy prior to an increase in α-syn accumulation. *A*, differentiated SH-SY5Y cells were treated with 1 μg/ml of Pam3CSK4 for 0, 4, or 8 days, and their lysates used for immunoblot-detection of total α-synuclein, TLR2, P62, LAMP2A, LC3B, and β-actin. For the cells treated for 8 days, the media were replaced at day 4 without addition of Pam3CSK4 in the media change. *B*, graphs represent the

potentiated levels of α-synuclein were still evident 6 days after dual stimulation with Pam3CSK4 plus PFF (Fig. 4, *E* and *F*).

TLR2 knockout ameliorates potentiated α-synuclein pathology in SH-SY5Y cells

To further confirm the role of TLR2 signaling in Pam3CSK4-induced autophagy blockade and subsequent α-synuclein pathology and to establish a proof of principle that TLR2 may be a therapeutic target for PD, we generated a TLR2 knockout SH-SY5Y cell line using CRISPR-Cas9 gene editing (Fig. S3). WT and TLR2 knockout SH-SY5Y cells were then differentiated and treated with the α-synuclein PFFs in the presence/absence of TLR2 agonist Pam3CSK4 using the same timepoints and concentrations as before. Again, both α-synuclein (Fig. 5, *A* and *B*) and P62 (Fig. 5, *C* and *D*) were significantly increased upon treatment with Pam3CSK4+PFF in the WT SH-SY5Y cells, but not the TLR2-knockout cells, confirming that Pam3CSK4 is acting *via* TLR2 and indicating that preventing TLR2 activation may be a therapeutic intervention for PD.

TLR2 activation potentiates α-synuclein pathology in human iPSC-derived neuronal cells

To confirm that TLR2 potentiation of α-synuclein pathology could also be seen in primary human neural cells, human skin fibroblasts from a patient with PD were reprogrammed into iPSCs that expressed pluripotency markers (SOX2, TRA1-60, SSEA4, and OCT4) (Fig. S4*A*) and then into neural progenitor cells, with >95% of the neural progenitor cells expressing Nestin (Fig. S4*B*). We then differentiated these cells into neurons that expressed TUJ1 and MAP2 (Fig. S4*C*). The IPS-derived neurons were then treated with or without Pam3CSK4 at 1 μg/ml for 4 days and then PFFs were added for another 48 h. As for SH-SY5Y cells, the protein levels of α-synuclein (Fig. 6, *A* and *B*) and P62 (Fig. 6, *C* and *D*) were both increased significantly in cells treated with both Pam3CSK4 and PFF together.

TLR2 inhibition ameliorates potentiated α-synuclein pathology in human iPSC-derived neuronal cells

Next, we aimed to determine if a novel small molecule antagonist of TLR2 (NPT1220–321) could ameliorate α-synuclein PFF pathology in Pam3CSK4-treated neural cells. To determine a dose of compound that could prevent TLR2 activation in neural cells, a dose–response experiment was first performed in SH-SY5Y cells using inflammatory cytokine gene expression as a readout. All three concentrations tested markedly suppressed the gene expression of as tumor necrosis factor α (Fig. 7*A*), IL-8 (Fig. 7*B*), and CCL5 (Fig. 7*C*) following stimulation of cells with Pam3CSK4. Subsequently, TLR2 antagonist concentrations of 1 and 3 μM were able to ameliorate TLR2-induced α-synuclein accumulation in SH-SY5Y cells (Fig. 7, *D* and *E*). Moreover, NPT1220-321 concentrations of one and 0.5 μM ameliorated α-synuclein accumulation in the differentiated iPSC-derived neurons (Fig. 7, *F* and *G*). To determine if TLR2 inhibition could also rescue TLR2-potential pathology, differentiated iPSC-derived neurons were treated in the presence/absence of NPT1220-312 at a concentration of 0.5 μM for 24 h prior to TLR2 agonist treatment with 1 μg/ml Pam3CSK4. PFFs were then added 4 days later, and cells maintained for another 2 days before fixing and staining. Once again, a significant increase in the levels of α-synuclein (Fig. 8, *A* and *B*) and P62 (Fig. 8, *C* and *D*) was observed in the cells treated with Pam3CSK4+PFF compared to the control, and this increase was significantly reduced with TLR2 antagonist treatment

Discussion

The outcomes of this study indicate that activation of TLR2 on neurons can contribute to the accumulation of the pathological PD protein α-synuclein. Within 48 h of neuronal TLR2 activation, increased lysosomal size and impaired autophagic flux could be measured. However, levels of α-synuclein did not increase until 6 to 8 days later, suggesting that a more prolonged defect in autophagy clearance is required for α-synuclein build up. Intriguingly, levels of LAMP2A, a measure of chaperone-mediated autophagy (CMA) were also increased at the same time as α-synuclein, indicating impaired CMA. Both CMA and macroautophagy are proposed to contribute to the clearance of wildtype α-synuclein protein in neurons (17). Thus, although our study focused on earlier events following TLR2 activation, it would be of future interest to determine if specific defects in CMA are a cause or consequence of the later time point accumulation of α-synuclein. In line with this, it would also be of interest to further characterize the accumulated α-synuclein, as different autophagy clearance pathways may be associated with specific pathological forms of α-synuclein (18, 19).

The temporal changes observed in autophagy pathway impairment and α-synuclein accumulation following neuronal TLR2 activation mimic what we and others have observed previously following seeding of neuronal cells with α-synuclein PFFs (16, 20). Thus, we investigated whether or not TLR2 activation could exacerbate α-synuclein pathology seeded with PFFs. Indeed, a marked potentiation of α-synuclein pathology was observed when PFFs were added to TLR2 stimulated

quantified expression of P62 and α-synuclein after correction to β-actin for loading. Data are represented as mean ± SEM and are expressed as fold-increase/β-actin from day 0. Representative data from at least n = 2 replicate experiments are shown. Differentiated SH-SY5Y cells were grown on coverslips and fixed after 0, 4, 8, or 12 days posttreatment with 1 μg/ml PamCSK4 for α-synuclein (*C*) and P62 (*D*) immunostaining (shown in *green*). Media were replaced at day 4 and 8 for the cells treated that long. Confocal images taken at 40× magnification are representative of the 4 to 6 images per condition containing 50 to 100 cells per image that were used for the analysis of α-synuclein intensity. Confocal images taken at 60× magnification with immersion oil are representative of the 8 to 12 images per condition, containing 15 to 40 cells per image that were used for the analysis of P62 intensity. *E*, graph shows quantified α-synuclein staining intensity as mean ± SEM. *F*, graph shows P62 staining intensity per cell as mean ± SEM. *G*, differentiated SH-SY5Y were treated with or without 1 μg/ml Pam3CSK4 and transduced with Premo Autophagy Tandem Sensor. The graph shows the percentage of RFP pixels colocalized with GFP pixels for different treatment conditions. *H*, graph represents the percentage of total LC3 puncta that are GFP + RFP+ or GFP-RFP+ for control and Pam3CSK4 treatment conditions. For all graphs $*p < 0.05$, $**p < 0.01$, $***p < 0.001$, $****p < 0.0001$. TLR2, toll-like receptor 2.

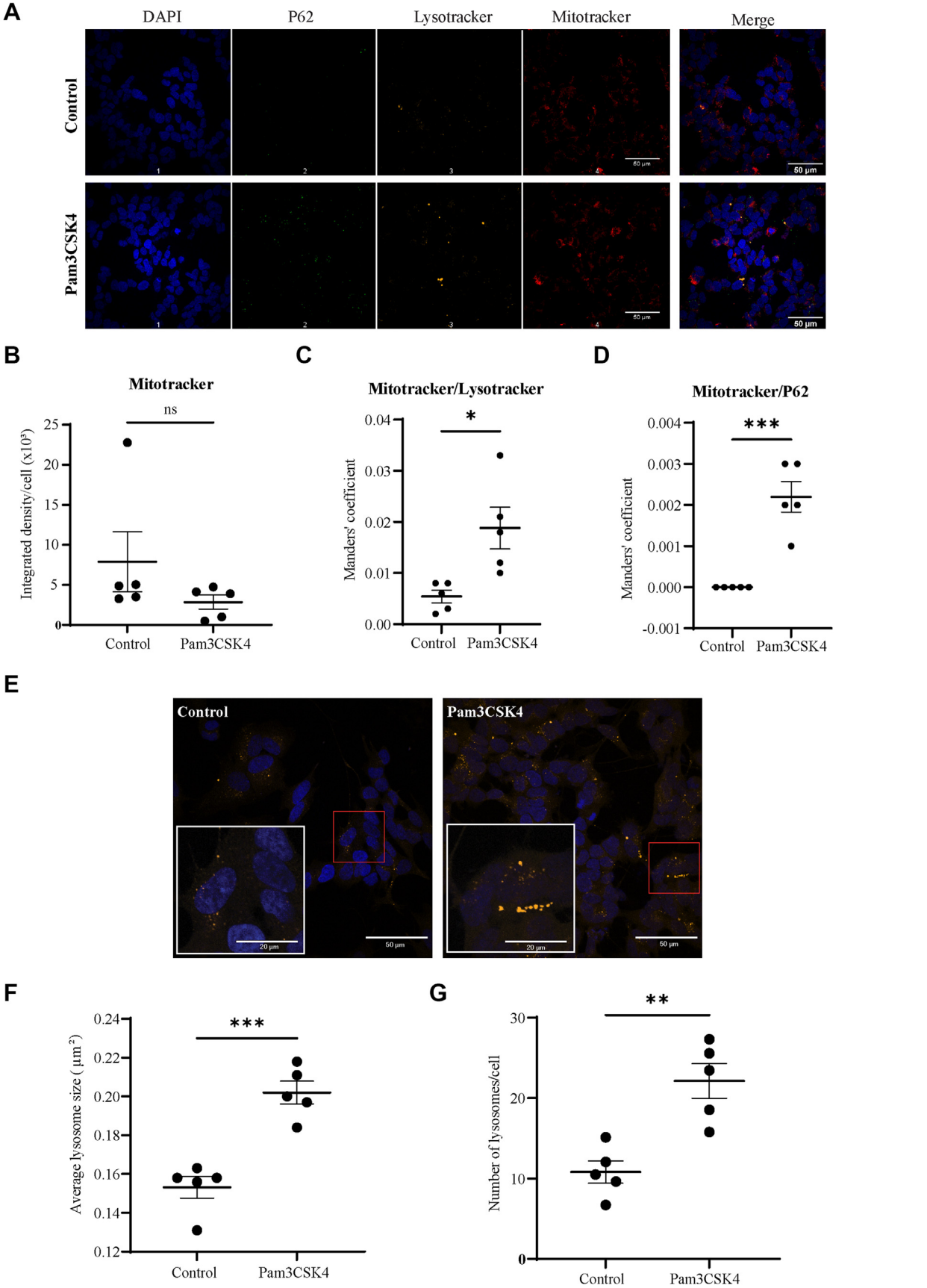

Figure 2. Neuronal TLR2 activation impairs multiple autophagy-lysosomal pathway measures. *A*, differentiated SH-SY5Y cells were grown on coverslips and fixed after 2 days posttreatment with 1 μg/ml PamCSK4 for P62 immunostaining (shown in *green*). One hour before fixing, Mitotracker *Deep Red* was used to stain mitochondria (shown in *red*), and Lysotracker Red DND-99 was used to stain lysosomes (shown in *orange*). Confocal images taken at 60×

neurons. This suggests that following TLR2 activation, levels of endogenous α-synuclein are increased, and the autophagic clearance of internalized exogenous α-synuclein is decreased, greatly facilitating the conditions needed to seed the pathological conversion of endogenous α-synuclein to pathogenic forms. This observation may provide support for a 2-hit model of PD, where an immune event triggering TLR2 activation could promote the cellular conditions needed for pathological α-synuclein formation. TLR2 activation also markedly upregulates the expression of TLR2 itself, which may also contribute to increased uptake of exogenous α-synuclein. However, we did not detect decreased uptake of PFF in TLR2-deficient SH-SY5Y cells. This is likely in agreement with studies indicating that TLR2 specifically interacts with oligomeric forms of α-synuclein rather than fibrils (21–23).

The upregulation of TLR2 in PD brain in association with α-synuclein pathology clearly indicates activation of the TLR2 pathway in PD brain (7). Preclinical studies with genetic rodent models further support that TLR2 inhibition is a potential disease modifying treatment for PD. Crossing A53T mutant α-synuclein with TLR2 knockout mice reduces neuronal α-synuclein levels in the substantia nigra (11). The same results were observed following lentiviral-mediated knockdown of TLR2 in mouse hippocampus (11). Lentiviral knockdown of TLR2 also improved motor symptoms of transgenic α-synuclein overexpressing mice, whilst overexpression of TLR2 promoted α-synuclein pathology and neurodegeneration (8). Neutralizing antibodies against TLR2 have also proven effective in reducing α-synuclein pathology in a mouse PD model (8). In the current study, we further demonstrate that TLR2-mediated pathology can be ameliorated with a small molecule TLR2 inhibitor in a human neural cell line and iPSC-derived neurons, further suggesting that pharmacological approaches inhibiting TLR2 may also be a tangible future therapeutic option for the treatment of PD.

Further work is still required to determine the exact signaling mechanisms leading to TLR2-mediated autophagy inhibition. Furthermore, it would be important to extend findings with the TLR2 inhibitor to human midbrain neural models, in order to determine the consequences for the dopaminergic cell death that underlies PD motor symptoms, as well as *in vivo* studies in appropriate preclinical models. It would also be of importance to determine the action of TLR2 inhibitors in mixed cultures of neurons and glia, as glia have a high expression of TLR2 and certainly contribute to PD pathology.

Experimental procedures

Materials

The NPT1220-321 TLR2 antagonist used in this study was kindly provided by Neuropore Therapies, and detailed characterization of this compound has been published elsewhere (24).

Tissue culture using SH-SY5Y cells

Human neuroblastoma SH-SY5Y cells were cultured in Dulbecco's modified Eagle medium/Hams F12 supplemented with 10% low endotoxin fetal bovine serum and 1 × penicillin/streptomycin solution (all from Gibco, Life Technologies). Cells were differentiated for 7 days in the same media except with 1% fetal bovine serum and 10 μM retinoic acid (Sigma), with media replaced every 2 days. Cells were treated with the TLR2 agonist Pam3CSK4 (Invivogen) and/or α-synuclein PFFs diluted in differentiation media at 1 μg/ml for time points as indicated.

Generation of knockout SH-SY5Y cells

To generate TLR2 knockout cells, 100 ng of predesigned GFP-tagged CRISPR-Cas9 plasmids with guide RNA sequences targeting human TLR2 (Horizon) were amplified in DH5α *E. coli* and purified using PureLink plasmid DNA purification kits (Thermo Fisher). A genomic cleavage detection kit (GeneArt, Thermo Fisher) was used according to the manufacturer's instructions to identify the plasmid most efficient at targeting and cleaving the TLR2 gene. The identified optimal CRISPR-Cas9 plasmid (2 μg) were then transfected into SH-SY5Y cells using Lipofectamine 3000 (Thermo Fisher). FACS (BD Influx) was used to plate successfully transfected GFP-positive cells into 96-well plates for clonal expansion. Expanded clones were screened for knockout by immunoblotting for TLR2 following a 48-h stimulation with 1 μg/ml Pam3CSK4 (Fig. S1). The generation of the α-synuclein knockout cells used in this study has been described previously (16).

Preparation of α-synuclein PFFs

Human recombinant α-synuclein monomeric protein at 13.2 mg/ml in 10 mM Tris and 50 mM NaCl, pH 7.6, was purchased from Proteos, and PFFs were prepared as recommended (25). Briefly, monomeric protein was diluted to 5 mg/ml in sterile Dulbecco's phosphate-buffered saline (Ca^{2+}-, Mg^{2+}-free; Gibco) and continuously shaken at 1000 rpm on an orbital shaker (Thermomix) placed in a 37 °C incubator for 7 days. The presence of amyloid fibrils was then confirmed by thioflavin T assay. Twenty-five microliter aliquots of resulting fibrillar α-synuclein were stored at −80 °C. Immediately before treating the cells, the fibrillar α-synuclein was diluted in sterile Dulbecco's phosphate-buffered saline to 0.1 mg/ml and sonicated for 2 min at 40% amplitude and 1-s on/off pulse durations (Q125, QSonica) to obtain a homogenous PFFs suspension for experiments as we have characterized previously (16).

magnification are representative of the 4 to 6 images per condition, containing 15 to 40 cells per image that were used for the analysis of staining intensity. *B*, graph shows staining intensity per cell of Mitotracker as mean ± SEM. *C* and *D*, graphs represent Manders' coefficient of colocalization respectively of Mitotracker with lysotracker (*C*) and Mitotracker with P62 (*D*). *E*, particle analysis was used to count the number of lysosomes per cell, and the average lysosome size using the Lysotracker stain. Confocal images showing enlarged lysosomes (*orange*) in differentiated SH-SY5Y cells treated with Pam3CSK4 for 2 days, compared to control. Images are taken at 60× magnification with immersion oil are representative of the 4 to 6 images per condition, containing 15 to 40 cells per image used for particle analysis of Lysotracker. *F*, graph shows the average lysosome surface area in μm^2 as mean ± SEM. *G*, graph shows the number of lysosomes per cell as mean ± SEM. For all graphs, * $p < 0.05$, ** $p < 0.01$, *** $p < 0.001$. TLR2, toll-like receptor 2.

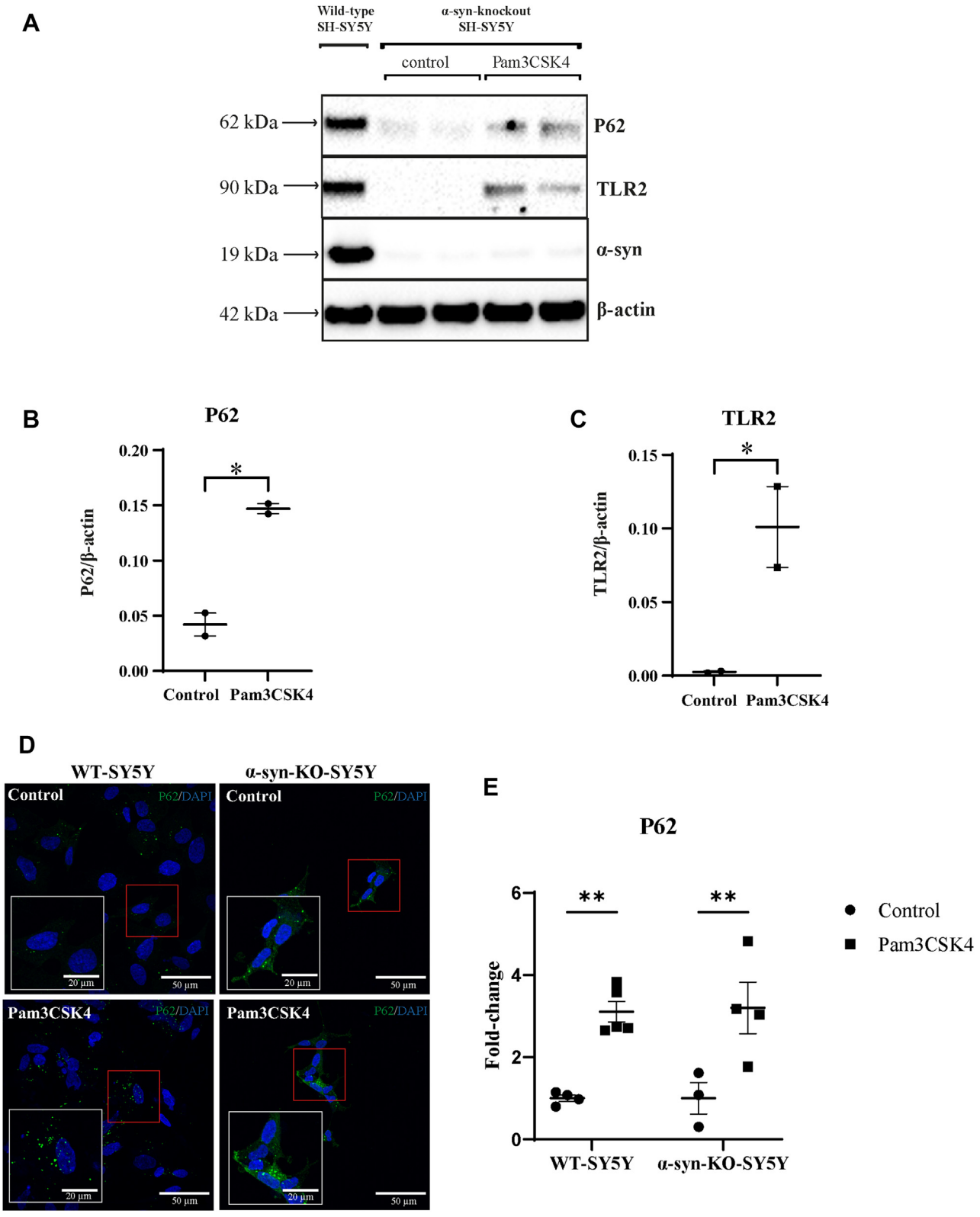

Figure 3. α-Synuclein is not required for TLR2-mediated autophagy inhibition. *A*, differentiated wildtype SH-SY5Y and α-synuclein KO SH-SY5Y cells were treated with 1 μg/ml Pam3CSK4 for 4 days and protein lysates collected for immunoblot of α-synuclein, TLR2, and P62. Graphs represent the quantified expression of P62 (*B*) and TLR2 (*C*) after correction to β-actin for loading. Data are represented as mean ± SEM and are expressed as quantified protein level/β-actin. Representative data from at least n = 3 independent experiments are shown. (Lane 1: protein lysates from wild type SH-SY5Y cells used as a positive control for α-synuclein). *D*, differentiated wildtype SH-SY5Y and α-synuclein-knockout SH-SY5Y cells were grown on coverslips and fixed 4 days posttreatment with 1 μg/ml PamCSK4 for P62 immunostaining (shown in *green*). Media were replaced at day 4 and 8 for the cells treated that long. Confocal images taken at 60× magnification with immersion oil are representative of the five images per condition, containing 15 to 40 cells per image that were used for the analysis of P62 intensity. *E*, graph shows quantified α-synuclein staining intensity as mean ± SEM. *$p < 0.05$, **$p < 0.01$. TLR2, toll-like receptor 2.

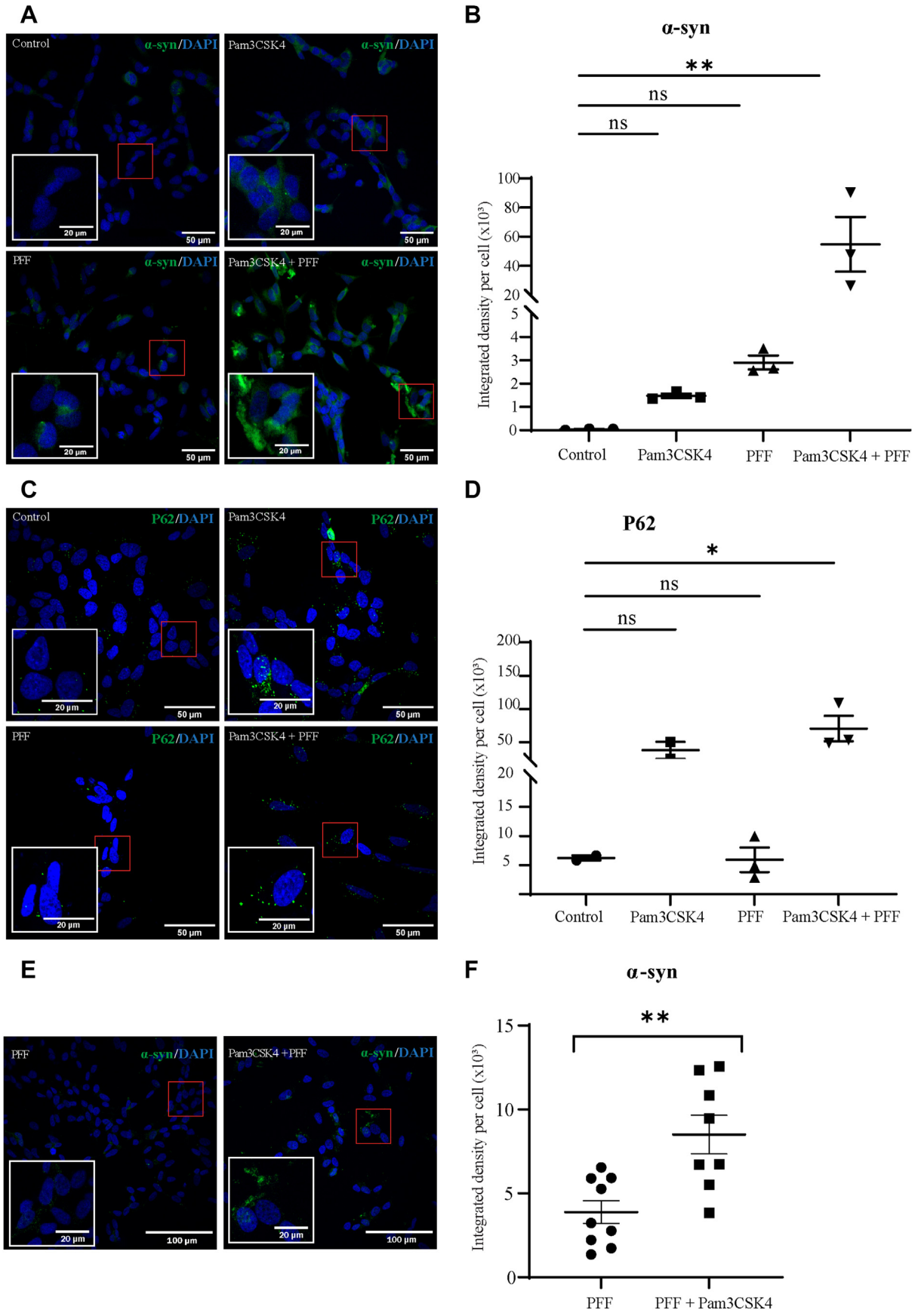

Figure 4. Neuronal TLR2 activation potentiates fibril-mediated pathology in SH-SY5Y cells. Differentiated SH-SY5Y cells were treated in the presence or absence of 1 μg/ml Pam3CSK4 for 4 days, then in the presence or absence of 1 μg/ml PFF for another 2 days and finally fixed for α-synuclein (*A* and *B*)

Generation and culture of PD patient iPSCs

Human fibroblasts from an idiopathic PD patient were obtained from the NINDS genetic repository at Coriell (#ND29494). Briefly, primary fibroblasts at passage four were reprogrammed to iPSCs using the EPi5 reprogramming kit (Life Technologies) as per the manufacturer instructions and as we have detailed before (7). Briefly, resulting iPSCs following reprogramming were maintained on Geltrex (Life Technologies)-coated dishes and stained for pluripotency markers (Pluripotent stem cell marker immunocytochemistry kit, Life Technologies) as per the manufacturer instructions. Neural progenitor cells were then derived from iPSCs using the PSC neural induction kit (Life Technologies) as per the manufacturer instructions with differentiation of neural progenitor cells confirmed by immunocytochemistry for Nestin. Neural stem cells were cultured in neural expansion medium composed of 50% advanced DMEM and 50% neurobasal medium supplemented with neural induction supplement at 1:50 dilution and 1× penicillin-streptomycin (all from Gibco, Thermo Fisher). The medium was changed every 2 days, and neural stem cells were passaged in the presence of 10 μl/ml RevitaCell supplement (Thermo Fisher). For the directed differentiation to neurons, neural progenitor cells were plated at a density of 1.5×10^4 cells per chamber on Nunc Lab-Tek II Chamber Slide System slides coated with poly-l-ornithine (Sigma) and laminin (10 μg/ml, Life Technologies). Cells were cultured in neurobasal media containing 2% B27 supplement and 2 mM Glutamax (all Life Technologies) for the first 3 days. After that, the media were changed to neurobasal media PLUS supplemented with 2% B27+ and 2 mM Glutamax (Life Technologies). Half of the media were replaced every second day. Cells were differentiated for 14 days prior to the commencement of experiments.

Immunoblot analysis

For immunoblot analysis, cells were lysed in buffer containing 50 mM Tris HCl pH 7.5, 1 mM EGTA, 1 mM EDTA, 1 mM sodium orthovanadate, 50 mM sodium fluoride, 5 mM sodium pyrophosphate, 0.27 M sucrose, 1 mM benzamadine, 1 mM phenylmethylsulphonyl fluoride, and 1% (v/v) Triton X-100. Lysates were then clarified by centrifugation at 13,000*g* for 20 min, and protein concentrations were measured by bicinchoninic acid assay (Pierce BCA Protein Assay Kit, Thermo Scientific), according to the manufacturer's instructions. Samples were stored at −80 °C until use. Up to 30 μg of protein lysate was heated with sample buffer (2% SDS, 20% glycerol, 2.5% bromophenol blue, 12.5 mM Tris–HCl, pH 6.8, 5% 2-mercaptoethanol) and separated by reducing SDS-PAGE before transfer to nitrocellulose membrane (Bio-Rad) (or PVDF in the case of LC3). Membranes were blocked in 5% skim milk dissolved in 1 × TBS-T (0.87% NaCl, 0.01 M Tris, pH 7.4, with 0.1% Tween20). Membranes were then cut into strips based on molecular weight markers and incubated overnight in primary antibodies prior to protein detection using horseradish peroxidase-conjugated secondary antibodies (Bio-Rad) with enhanced chemiluminescence substrate (Amersham ECL Plus Western Blot Detection System, GE Healthcare). Primary antibodies for immunoblotting were rabbit monoclonal TLR2 (Abcam, 1:500 dilution), mouse monoclonal α-synuclein (BD Biosciences, 1:3000 dilution), mouse monoclonal p62/SQSTM1 (Abcam, 1:1000 dilution), rabbit polyclonal LC3B (Novus biologicals, 1:1000 dilution), rabbit polyclonal LAMP2A (Abcam, 1:1000 dilution), and β-actin (Abcam, 1:50,000 dilution) used as a protein loading control. Antibody catalog numbers are provided in Table S1. A Bio-Rad Chemidoc MP system was used to capture images, and the relative levels of each protein of interest were analyzed using Image J software (US National Institutes of Health). The intensity of each protein band was quantified and expressed as arbitrary units standardized to β-actin.

Immunocytochemistry

For immunocytochemistry, cells cultured on either coverslips (SHSY5Y cells) or in chamber slides (iPSC-derived neurons), were washed in 1 × PBS, and fixed in 4% paraformaldehyde for 15 min at room temperature. Coverslips were washed again in 1 × PBS after fixing and permeabilized with 0.3% Triton X-100 for 20 min. Cells were then blocked in 3% BSA for 1 h and incubated overnight at 4 °C in primary antibody at a dilution of 1:400 in 3% BSA. Primary antibodies used were mouse monoclonal α-synuclein (BD biosciences, 1:400 dilution), mouse monoclonal P62/SQSTM1 (Abcam, 1:400 dilution), rabbit monoclonal MAP2 (Abcam, 1:400 dilution), and rabbit monoclonal TUJ1 (Abcam, 1:400 dilution). Antibody catalog numbers are provided in Table S1. After incubation, cells were washed 3 × 5 min in 1 × PBS and incubated with Alexa Fluor secondary antibodies (Abcam, 1:400 dilution) in 3% BSA for 1 h at room temperature in the dark. Cells were washed again for 3 × 5 min in 1 × PBS with DAPI added to the last wash at a concentration of 1:10,000. Coverslips were mounted face down using fluorescent mounting medium (Dako), and chamber slides were mounted with rectangular coverslips. Slides were left to dry in the dark for 24 h before visualizing. Images were captured on a confocal microscope (Nikon) using NIS elements AR software with optical configuration settings kept constant for all images.

Detection of lysosomes, autophagosomes, autolysosomes, and mitochondria

Differentiated SH-SY5Y cells were cultured in 96-wells plate at 10,000 cells per well and treated with or without

and P62 (*C* and *D*) immunostaining (shown in *green*). The media were replaced at day 4 without adding Pam3CSK4 or PFF. Confocal images taken at 40× magnification are representative of the 4 to 6 images per condition containing 50 to 100 cells per image that were used for the analysis of α-synuclein intensity. Confocal images taken at 60× magnification with immersion oil are representative of the 4 to 6 images per condition containing 15 to 40 cells per image that were used for the analysis of P62 intensity. Graphs show staining intensity as mean ± SEM. *E*, differentiated SH-SY5Y cells were treated in the presence or absence of 1 μg/ml Pam3CSK4 for 4 days, then with 1 μg/ml PFF for another 6 days and finally fixed for α-synuclein immunostaining (shown in *green*). The media were replaced at day 4 without adding Pam3CSK4 or PFF. Confocal images taken at 40× magnification are representative of the 4 to 6 images per condition containing 50 to 100 cells per image that were used for the analysis of α-synuclein intensity. *F*, graph shows staining intensity as mean ± SEM. For all graphs, * $p < 0.05$, ** $p < 0.01$. PFF, preformed fibril; TLR2, toll-like receptor 2.

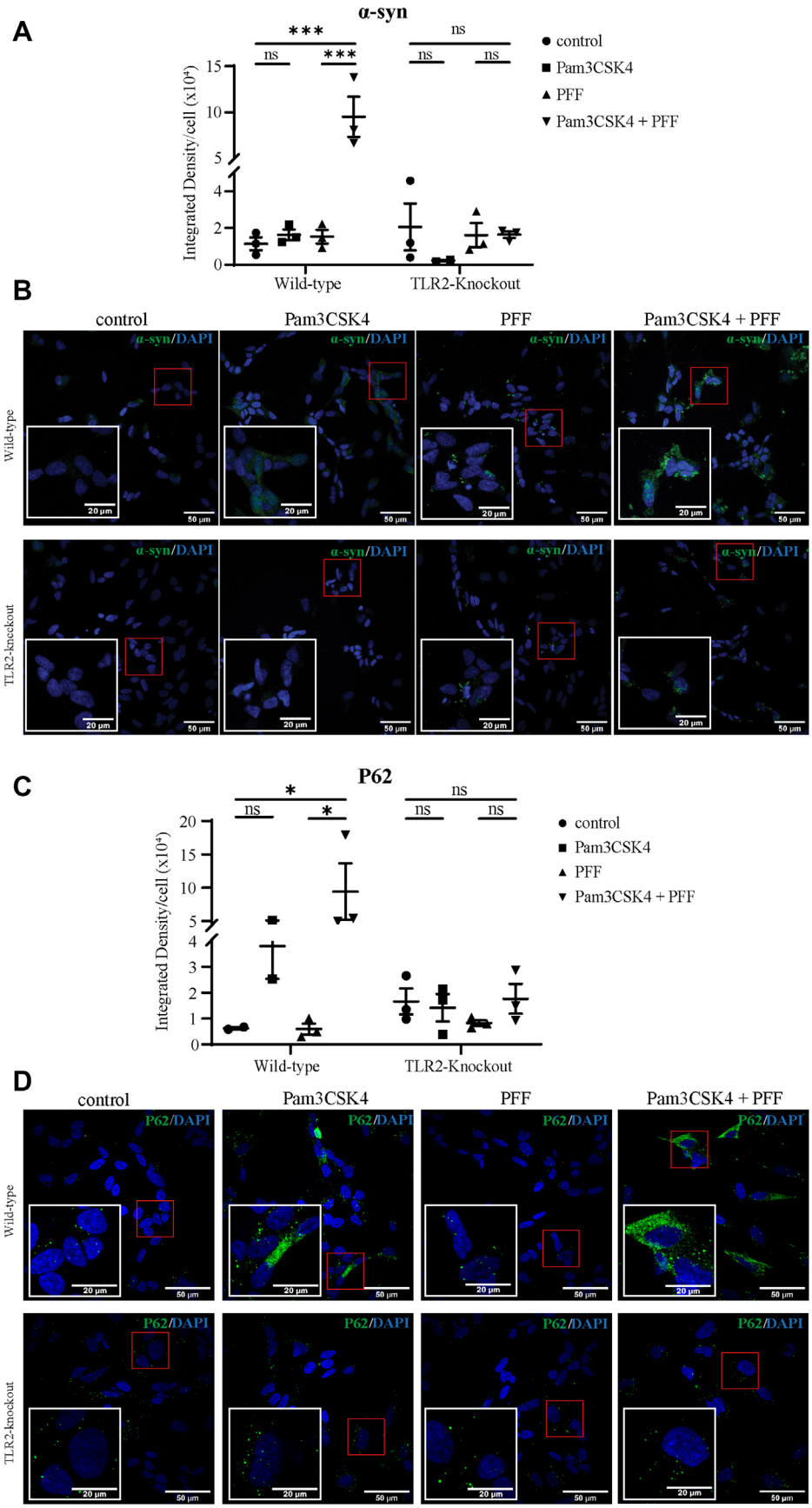

Figure 5. TLR2–mediated PFF potentiated pathology is ameliorated in TLR2 KO neural cells. *A*, differentiated wildtype and TLR2 KO SH-SY5Y cells were treated in the presence or absence of 1 μg/ml Pam3CSK4 for 4 days, then in the presence or absence of 1 μg/ml PFF for another 2 days and finally fixed for α-synuclein (*A* and *B*) and P62 (*C* and *D*) immunostaining (shown in *green*). The media were replaced at day 4 without adding Pam3CSK4 or PFF. Confocal

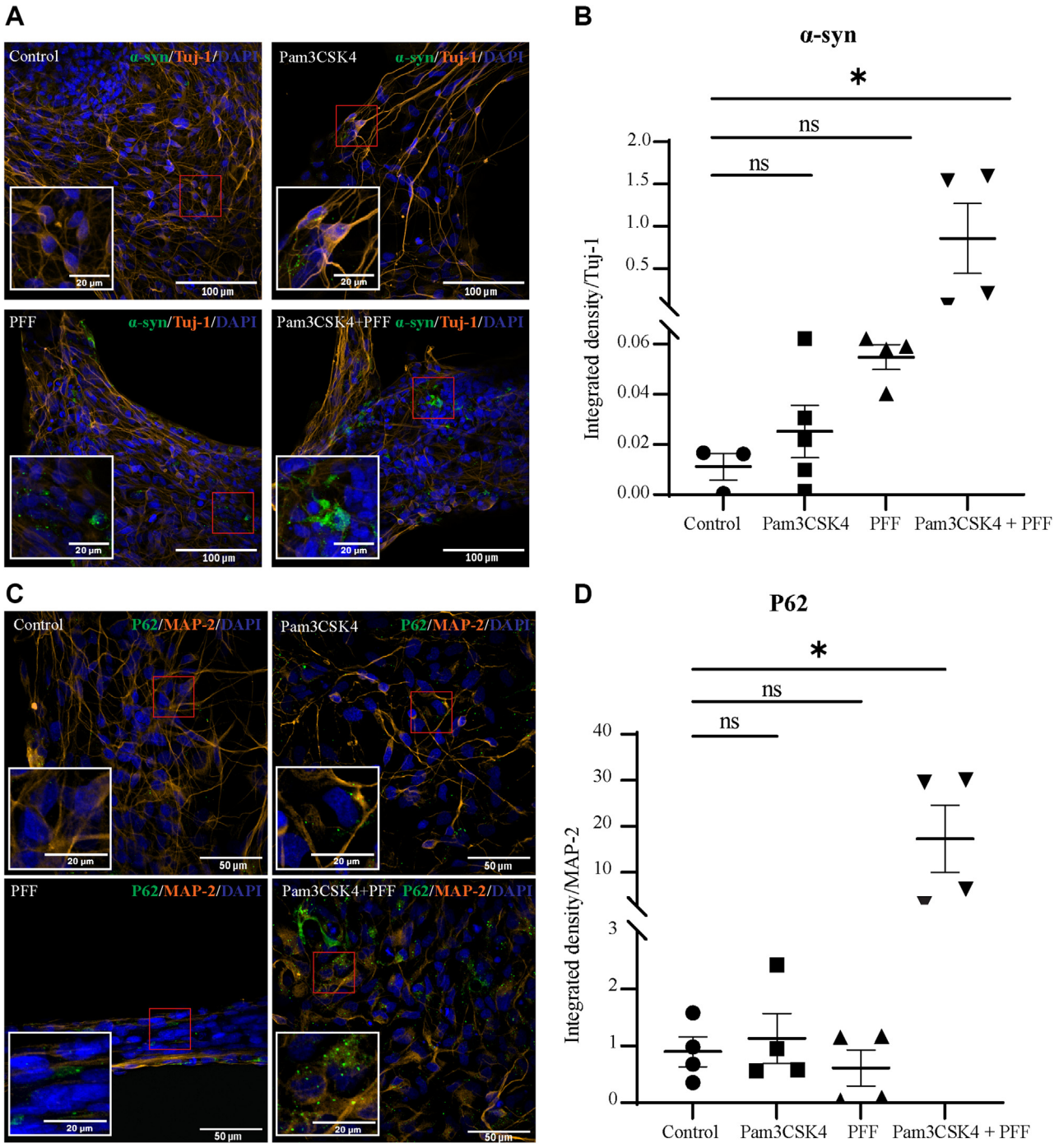

Figure 6. Neuronal TLR2 activation potentiates α-synuclein fibril pathology in iPSC-derived neurons. iPSC-derived neural stem cells were differentiated into neurons and cultured for 4 days with or without 1 μg/ml Pam3CSK4 and for another 2 days with or without 1 μg/ml PFFs. *A*, cells were fixed and stained for total α-synuclein (*green*) and TUJ1 (*orange*). Confocal images were taken at 40× magnification. Four to six images were captured per condition, each containing 50 to 200 cells, and used for the analysis of α-synuclein intensity. *B*, graph shows α-synuclein intensity/TUJ1 as mean ± S.E.M. *C*, cells were fixed and stained for total P62 (*green*) and MAP2 (*orange*). Confocal images were taken at 60× magnification with immersion oil. Four to six images were captured per condition, each containing 60 to 100 cells, and used for the analysis of P62 intensity. *D*, graph shows P62/MAP2 as mean ± S.E.M. For all graphs $^{*}p < 0.05$. iPSCs, induced pluripotent stem cells; PFF, preformed fibril; TLR2, toll-like receptor 2.

Pam3CSK4 for 2 days in the presence or absence of lysosomal inhibitor chloroquine, which was added for the last 24 h at a concentration of 20 μM. Twenty-four hours prior to imaging, Premo Autophagy Tandem Sensor reagent (Thermo Fisher) was added at 2 μl/10^4 cells yielding an average of 40 particles per cell. Finally, the nuclei were

images taken at 40× magnification are representative of the 4 to 6 images per condition containing 50 to 100 cells per image that were used for the analysis of α-synuclein intensity. Confocal images taken at 60× magnification with immersion oil are representative of the 4 to 6 images per condition containing 15 to 40 cells per image that were used for the analysis of P62 intensity. Graphs show staining intensity as mean ± SEM. For all graphs, $^{*}p < 0.05$, $^{***}p < 0.001$. PFF, preformed fibril; TLR2, toll-like receptor 2.

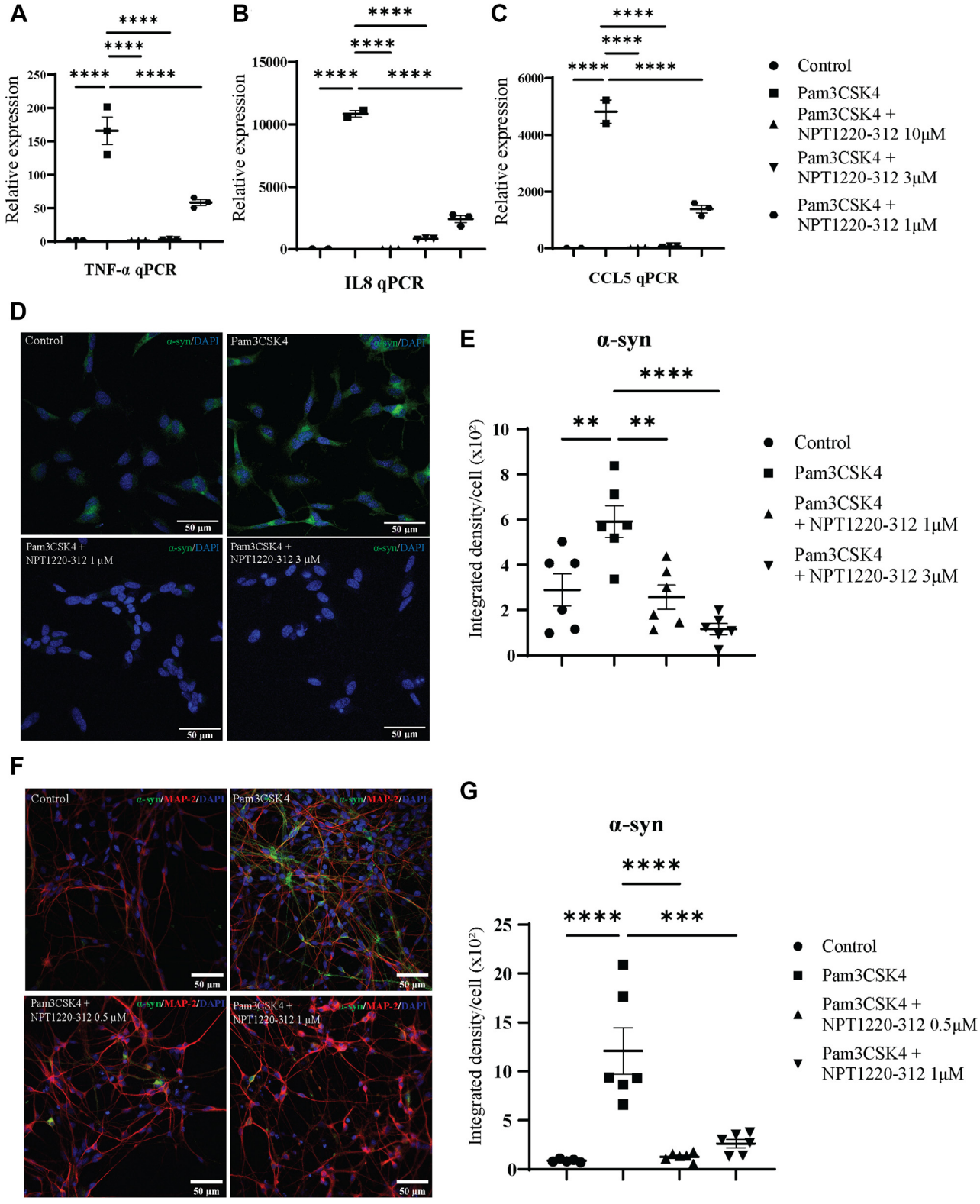

Figure 7. TLR2–mediated PFF potentiated pathology is ameliorated with a small molecule TLR2 inhibitor. Cells were treated with 1 μg/ml Pam3CSK4 for 8 h in the absence or presence of TLR2 inhibitor NPT1220-312 at concentrations of 10 μM, 3 μM, and 1 μM. mRNA was then extracted for real-time qPCR measurement of TNFα (*A*), IL-8 (*B*), and CCL5 (*C*). Relative gene expression was calculated using the 2-ddct method with GAPDH as the housekeeping gene. Graphs show mean relative expression ± SEM. *D*, differentiated SH-SY5Y cells were treated with or without 1 μg/ml Pam3CSK4 in the presence or absence of NPT1220-312 at 1 μM or 3 μM, for 7 days and fixed for α-synuclein immunostaining (shown in *green*). Confocal images taken at 60× magnification with immersion oil are representative of the 4 to 6 images per condition containing 20 to 50 cells per image that were used for the analysis of staining intensity. *E*, graph shows staining intensity as mean ± SEM. *F*, iPSC-derived neural stem cells were differentiated into neurons and cultured for 7 days with or without 1 μg/ml Pam3CSK4 in the presence or absence of NPT1220-312 at 0.5 μM or 1 μM. Cells were fixed and stained for total α-synuclein (*green*) and MAP2 (*red*). *G*, graph shows staining intensity as mean ± SEM. For all graphs, $^{**}p < 0.01$, $^{***}p < 0.001$, $^{****}p < 0.0001$. TNFα, tumor necrosis factor α; iPSCs, induced pluripotent stem cells; PFF, preformed fibril; TLR2, toll-like receptor 2.

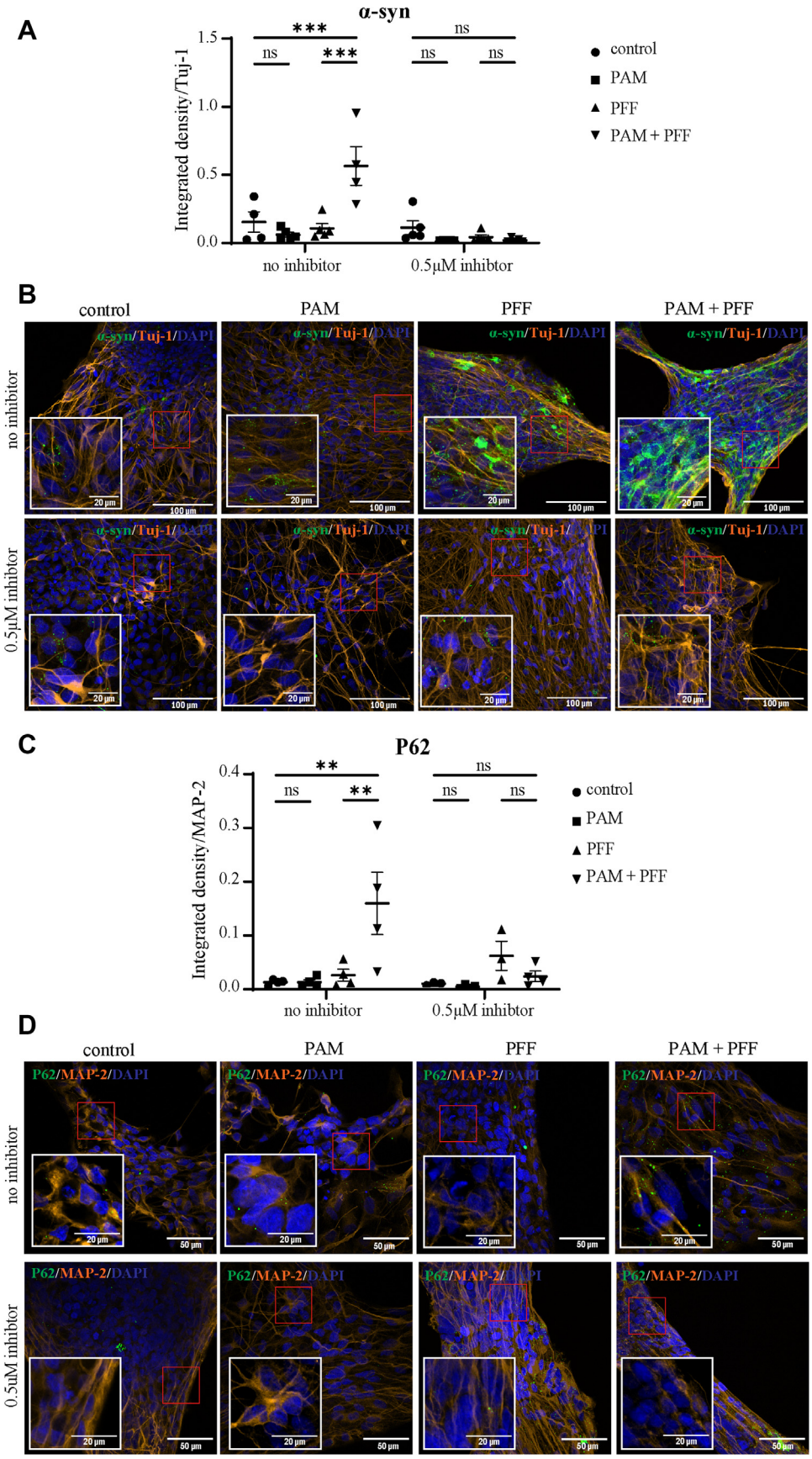

Figure 8. TLR2 inhibition ameliorates potentiated α-synuclein pathology in human iPSC-derived neuronal cells. *A*, differentiated iPSC-derived neurons were grown on 8-well chamber slides (Nunc Lab Tek II), treated with/without TLR2 inhibitor NPT-312 for 24 h. Pam3CSK4 was added, and 4 days later PFF treatment was done. Two days later, cells were fixed for α-synuclein immunostaining (shown in *green*). Cells were also co-stained with

stained using Hoesht 33,342, and cells were imaged using the Opera Phenix High-Content Screening System (PerkinElmer). On average, 500 cells (250 cells per well in duplicates) were imaged per condition and analyzed using Harmony software (PerkinElmer Inc.). For lysosome and mitochondria labeling, differentiated SH-SY5Y cells were plated onto Geltrex-coated coverslips in 12-wells plates and treated with or without Pam3CSK4 for 2 days. Cells were then incubated with Lysotracker Red DND-99 (Thermo Fisher) and Mitotracker Deep Red (Thermo Fisher) for 1 h at 37 °C before fixing and staining with DAPI. Cells were imaged with a confocal microscope (C2, Nikon) using NIS elements AR software with intensity settings kept constant for all images.

Image analysis

Confocal images obtained at 40× objective magnification were used for the analysis of α-synuclein in combination with Fiji ImageJ, whereas images obtained at 60× objective magnification were used to analyze intensity of autophagy marker p62, the Mitotracker, and Lysotracker probes and for the GFP-RFP-LC3 tandem autophagy sensor. For intensity analysis, the threshold tool was used to highlight all stained areas in the field, and the integrated density was measured. Cell number was counted for each image based on DAPI staining. Cells touching the edges of the image were excluded from the final analysis. Four to eight images containing 50 to 100 cells per image were analyzed for each treatment condition. Fluorescent intensity was then normalized to DAPI count for SH-SY5Y cells and either MAP2 or TUJ1 for IPS-derived neurons. For lysosome number and size analysis, the threshold tool was used to highlight lysotracker-labeled lysosomes, and particle analysis was performed to assess the number of lysosomes per cell and the average lysosome size in μm^2, and at least five images containing 25 to 60 cells per image each were analyzed per treatment condition. Colocalization analysis of Mitotracker, Lysotracker, and P62 were performed using the Coloc 2 function in Fiji. Manders' coefficient was calculated and expressed as the fraction of a marker that colocalizes with a second marker. For the analysis of GFP-RFP-LC3 tandem autophagy sensor, at least 16 fields of view containing 6 to 10 cells for each well were analyzed. The total number of RFP+ puncta per cell was computed, as well the respective percentages of GFP + RFP+ and GFP-RFP+ for each condition and the percentage of RFP pixels overlapping with GFP pixels. GFP and RFP fluorescence was measured with the Find Spots method using detection sensitivity settings of 0.29 and 0.21 and splitting sensitivity settings of 0.91 and 0.61, respectively

Gene expression

Inflammatory cytokine gene expression was measured as we have done previously (7). Briefly, RNA was extracted using the ReliaPrep miniprep system (Promega) and reverse transcribed to cDNA using the iScript cDNA synthesis kit (Bio-Rad). qRT-PCR was performed on a QuantStudio six Flex Real-Time PCR System (Life Technologies) using SYBR Green (Bio-Rad) in triplicate. Gene expression was quantified using the comparative Ct method with glyceraldehyde-3-phosphate dehydrogenase used as the housekeeping gene.

Statistical analysis

Statistical analysis was performed with Prism (GraphPad Software), which was also used to generate graphs. Student's *t* test was used for comparisons between two groups, one-way ANOVA with Tukey's post hoc test was used for comparisons between multiple conditions, and two-way ANOVA with multiple comparisons was used for grouped data. Statistical significance was set as $p < 0.05$, and data are presented as mean ± S.E.M. in the figures.

Data availability

All data generated are contained within the manuscript and supporting information.

Supporting information—This article contains supporting information.

Acknowledgments—The authors acknowledge the technical and scientific assistance of Sydney Microscopy & Microanalysis, the University of Sydney node of Microscopy Australia.

Author contribution—N. D. conceptualization; N. D. methodology; N. D., J. C., and A. L.-G. formal analysis; N. D., W. S. K., and G. M. H. writing-review and editing; J. C., A. L.-G., S. Z., J. G., Y. Z., and G. P. investigation; J. C. and A. L.-G. writing-original draft.

Funding and additional information—This study was supported by the National Health and Medical Research Council (NHMRC) of Australia, grant number 1103757. G. M. H. holds a NHMRC senior leadership fellowship (#176607). The Dementia and Movement Disorders Laboratory is supported by ForeFront, a collaborative research group dedicated to the study of non-Alzheimer disease degenerative disorders, funded by NHMRC grants (#1037746, #1095127, and #1132524).

Conflict of interest—The authors declare that they have no conflicts of interest with the contents of this article.

Abbreviations—The abbreviations used are: CMA, chaperone-mediated autophagy; iPSC, induced pluripotent stem cell; LBs, Lewy

neural marker TUJ1 (shown in *orange*) and nuclei counterstained with DAPI. Confocal images taken at 40× magnification are representative of the 3 to 6 images per condition containing 100 to 200 cells per image that were used for the analysis of staining intensity. α-synuclein expression level was normalized to TUJ1 expression level. *B*, the graph shows staining intensity of α-synuclein/TUJ1 as mean ± SEM. *C*, iPSC-derived neurons were grown on 8-well chamber slides (Nunc Lab Tek II), treated with/without TLR2 inhibitor NPT-312 for 24 h. Pam3CSK4 was added, and 4 days later, PFF treatment was done. Two days later cells were fixed for P62 immunostaining (shown in *green*). Cells were also co-stained with neural marker MAP2 (shown in *orange*) and nuclei counterstained with DAPI. Confocal images taken at 60× magnification are representative of the 3 to 6 images per condition containing 70 to 150 cells per image that were used for the analysis of staining intensity. *D*, the graph shows the staining intensity of P62/MAP2 as mean ± SEM. $^{**}p < 0.01$, $^{***}p < 0.001$. iPSCs, induced pluripotent stem cells; PFF, preformed fibril; TLR2, toll-like receptor 2.

bodies; PD, Parkinson's disease; PFF, preformed fibril; RFP, red fluorescent protein; TLR2, toll-like receptor 2.

References

1. Schneider, S. A., and Obeso, J. A. (2015) Clinical and pathological features of Parkinson's disease. *Curr. Top Behav. Neurosci.* **22**, 205–220
2. Baba, M., Nakajo, S., Tu, P. H., Tomita, T., Nakaya, K., Lee, V. M., *et al.* (1998) Aggregation of alpha-synuclein in Lewy bodies of sporadic Parkinson's disease and dementia with Lewy bodies. *Am. J. Pathol.* **152**, 879–884
3. Mueller, J. C., Fuchs, J., Hofer, A., Zimprich, A., Lichtner, P., Illig, T., *et al.* (2005) Multiple regions of alpha-synuclein are associated with Parkinson's disease. *Ann. Neurol.* **57**, 535–541
4. Braak, H., Del Tredici, K., Rub, U., de Vos, R. A., Jansen Steur, E. N., and Braak, E. (2003) Staging of brain pathology related to sporadic Parkinson's disease. *Neurobiol. Aging* **24**, 197–211
5. Medzhitov, R. (2001) Toll-like receptors and innate immunity. *Nat. Rev. Immunol.* **1**, 135–145
6. Kawai, T., and Akira, S. (2010) The role of pattern-recognition receptors in innate immunity: update on toll-like receptors. *Nat. Immunol.* **11**, 373–384
7. Dzamko, N., Gysbers, A., Perera, G., Bahar, A., Shankar, A., Gao, J., *et al.* (2017) Toll-like receptor 2 is increased in neurons in Parkinson's disease brain and may contribute to alpha-synuclein pathology. *Acta Neuropathol.* **133**, 303–319
8. Kim, C., Spencer, B., Rockenstein, E., Yamakado, H., Mante, M., Adame, A., *et al.* (2018) Immunotherapy targeting toll-like receptor 2 alleviates neurodegeneration in models of synucleinopathy by modulating α-synuclein transmission and neuroinflammation. *Mol. Neurodegener.* **13**, 43
9. Dutta, D., Jana, M., Majumder, M., Mondal, S., Roy, A., and Pahan, K. (2021) Selective targeting of the TLR2/MyD88/NF-κB pathway reduces α-synuclein spreading *in vitro* and *in vivo*. *Nat. Commun.* **12**, 5382
10. Xia, Y., Zhang, G., Kou, L., Yin, S., Han, C., Hu, J., *et al.* (2021) Reactive microglia enhance the transmission of exosomal alpha-synuclein *via* toll-like receptor 2. *Brain* **144**, 2024–2037
11. Kim, C., Rockenstein, E., Spencer, B., Kim, H. K., Adame, A., Trejo, M., *et al.* (2015) Antagonizing neuronal toll-like receptor 2 prevents synucleinopathy by activating autophagy. *Cell Rep.* **13**, 771–782
12. Larsen, K. E., and Sulzer, D. (2002) Autophagy in neurons: a review. *Histol. Histopathol.* **17**, 897–908
13. Hou, X., Watzlawik, J. O., Fiesel, F. C., and Springer, W. (2020) Autophagy in Parkinson's disease. *J. Mol. Biol.* **432**, 2651–2672
14. Moors, T. E., Hoozemans, J. J., Ingrassia, A., Beccari, T., Parnetti, L., Chartier-Harlin, M.-C., *et al.* (2017) Therapeutic potential of autophagy-enhancing agents in Parkinson's disease. *Mol. Neurodegener.* **12**, 11
15. Bonam, S. R., Tranchant, C., and Muller, S. (2021) Autophagy-lysosomal pathway as potential therapeutic target in Parkinson's disease. *Cells* **10**, 3547
16. Gao, J., Perera, G., Bhadbhade, M., Halliday, G. M., and Dzamko, N. (2019) Autophagy activation promotes clearance of alpha-synuclein inclusions in fibril-seeded human neural cells. *J. Biol. Chem.* **294**, 14241–14256
17. Vogiatzi, T., Xilouri, M., Vekrellis, K., and Stefanis, L. (2008) Wild type α-synuclein is degraded by chaperone-mediated autophagy and macroautophagy in neuronal cells. *J. Biol. Chem.* **283**, 23542–23556
18. Lee, H. J., Khoshaghideh, F., Patel, S., and Lee, S. J. (2004) Clearance of alpha-synuclein oligomeric intermediates *via* the lysosomal degradation pathway. *J. Neurosci.* **24**, 1888–1896
19. Lee, H.-J., and Lee, S.-J. (2002) Characterization of cytoplasmic α-synuclein aggregates: Fibril formation is tightly linked to the inclusion-forming process in cells. *J. Biol. Chem.* **277**, 48976–48983
20. Pantazopoulou, M., Brembati, V., Kanellidi, A., Bousset, L., Melki, R., and Stefanis, L. (2021) Distinct alpha-Synuclein species induced by seeding are selectively cleared by the Lysosome or the Proteasome in neuronally differentiated SH-SY5Y cells. *J. Neurochem.* **156**, 880–896
21. Kim, C., Ho, D.-H., Suk, J.-E., You, S., Michael, S., Kang, J., *et al.* (2013) Neuron-released oligomeric α-synuclein is an endogenous agonist of TLR2 for paracrine activation of microglia. *Nat. Commun.* **4**, 1562
22. Daniele, S. G., Beraud, D., Davenport, C., Cheng, K., Yin, H., and Maguire-Zeiss, K. A. (2015) Activation of MyD88-dependent TLR1/2 signaling by misfolded alpha-synuclein, a protein linked to neurodegenerative disorders. *Sci. Signal.* **8**, ra45
23. Scheiblich, H., Bousset, L., Schwartz, S., Griep, A., Latz, E., Melki, R., *et al.* (2021) Microglial NLRP3 inflammasome activation upon TLR2 and TLR5 ligation by distinct α-synuclein assemblies. *J. Immunol.* **207**, 2143–2154
24. Habas, A., Reddy Natala, S., Bowden-Verhoek, J. K., Stocking, E. M., Price, D. L., Wrasidlo, W., *et al.* (2022) NPT1220-312, a TLR2/TLR9 small molecule antagonist, inhibits pro-inflammatory signaling, cytokine release and NLRP3 inflammasome activation. *Int. J. Inflam.* https://doi.org/10.1155/2022/2337363
25. Polinski, N. K., Volpicelli-Daley, L. A., Sortwell, C. E., Luk, K. C., Cremades, N., Gottler, L. M., *et al.* (2018) Best practices for generating and using alpha-synuclein pre-formed fibrils to model Parkinson's disease in rodents. *J. Parkinsons. Dis.* **8**, 303–322